



HAL
open science

Semi-analytical computation of a quasi-static field induced by an eddy current probe in a conductor with a rough surface

François Caire, Denis Prémel, Gérard Granet

► To cite this version:

François Caire, Denis Prémel, Gérard Granet. Semi-analytical computation of a quasi-static field induced by an eddy current probe in a conductor with a rough surface. *European Physical Journal: Applied Physics*, 2013, 64, pp.24511. 10.1051/epjap/2013120400 . cea-01779418

HAL Id: cea-01779418

<https://cea.hal.science/cea-01779418>

Submitted on 28 Apr 2021

HAL is a multi-disciplinary open access archive for the deposit and dissemination of scientific research documents, whether they are published or not. The documents may come from teaching and research institutions in France or abroad, or from public or private research centers.

L'archive ouverte pluridisciplinaire **HAL**, est destinée au dépôt et à la diffusion de documents scientifiques de niveau recherche, publiés ou non, émanant des établissements d'enseignement et de recherche français ou étrangers, des laboratoires publics ou privés.

Semi-analytical computation of a quasi-static field induced by an eddy current probe in a conductor with a rough surface^{*}

François Caire^{1,a}, Denis Prémel¹, and Gérard Granet²

¹ CEA, LIST, Laboratoire de Simulation et Modélisation, 91191 Gif-sur-Yvette Cedex, France

² Institut Pascal, Université Blaise Pascal, France

Received: 27 September 2012 / Received in final form: 4 December 2012 / Accepted: 10 April 2013
Published online: 6 November 2013 – © EDP Sciences 2013

Abstract. Semi-analytical models developed at Cea List for the simulation of Eddy current non-destructive testing are currently based on the volume integral equation formalism. This method is very effective for canonical geometries such as planes or cylinders since the analytical expressions of Green's dyads are known. This approach requires three steps: the computation of the quasi-static fields induced by the probe in the workpiece without flaw, the determination of the interaction between the primary field and the defect and finally, the calculation of the response of the eddy current sensor, resulting from this interaction. In order to generalize this approach to more complex configurations, in this paper, we focus on the first step: the computation of quasi-static fields induced by an eddy current probe in a conductor with a rough surface. The semi-analytical model we generalize here is based on Maxwell's equations, written in a non-orthogonal coordinate system resulting in the writing of the boundary conditions at the interface by using a simple analytical expression. Starting from the second-order vector-potential formalism dedicated to non-orthogonal curvilinear coordinate systems, two scalar potentials are expressed as a modal expansion, satisfying the outgoing wave condition. Finally, the coefficients of the modal expansion are determined by applying boundary conditions at the complex interface. First numerical results, obtained considering a specific configuration, are compared to other Finite Element data.

Introduction

During the last decades, fast semi-analytical models, based on volume integral equations and Green's dyads formalism, have been developed for the simulation of the Eddy current non-destructive testing (ECNDT) of conductive pieces. The advantage of such approaches lies in the fact that the analytical expressions of the dyads are well known for canonical geometries like planes or cylinders and for stratified media. Besides, corresponding boundary conditions are directly included in the expression of the dyads. As a matter of fact, the computation times in these particular configurations are smaller than those obtained by a standard finite element method (FEM).

However, the analytical expression of the Green's dyads is not known for complex geometries, so if one wants to avoid the use of a purely numerical method in such cases, it is necessary to focus on another approach for an efficient simulation. Although the use of a boundary element method [1] can give the solution of such complex problems, we propose in this paper to generalize an original method based on a differential formalism.

^{*} Contribution to the Topical Issue "Numelec 2012", Edited by Adel Razek.

^a e-mail: francois.caire@cea.fr

The Curvilinear Coordinate Method or "C method" is widely used in the community of Applied Optics since it has been introduced by Chandezon et al. [2,3], and remains one of the most efficient methods for the computation of fields scattered by a diffraction grating enlightened by a plane wave. We propose here an extension of the configurations solved by this method, as we transpose it for the computation of quasi-static fields induced in a conductive material with a non-periodical rough surface, which is excited by an eddy current air-core probe (see Fig. 1). This extension has already been implemented for a pure 2D configuration [4], which has highlighted the accuracy and efficiency of the C method for solving eddy-current problems.

The main idea of the C method is to choose a coordinate system, such that the boundary concurs with the coordinate fitting the locally perturbed shape. As a consequence of this change of coordinate system, the analytical equation of the surface becomes more simple and allows us to treat the boundary conditions analytically. Maxwell's equations appear under the covariant form [5] in this new coordinate system and a new metric must be considered, as we shall see. Then, a proper decomposition of these equations [6] and the introduction of two scalar potentials yield an eigenvalue problem which is the direct

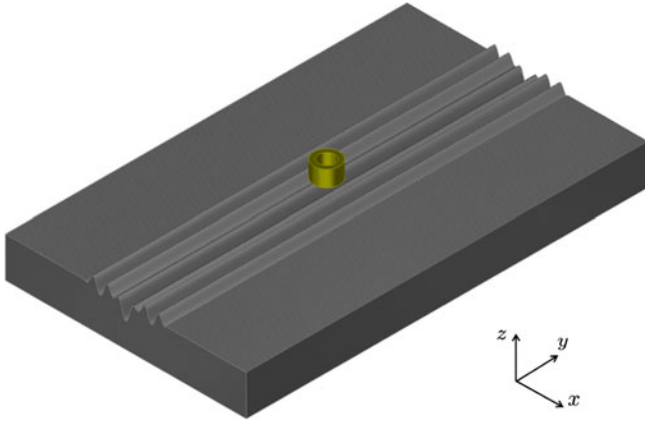


Fig. 1. General configuration considered: a coil inspecting a conductive half-space presenting an uneven surface varying along the x direction.

transcription of covariant Maxwell's equations without source terms. Thus, the unknown potentials are expanded as linear combinations (one in each medium) of eigenvectors in which the weight coefficients remain unknown. To determine them, we introduce the field created by the probe in air and we apply the boundary conditions on the surface. From the potentials, it is then easy to reconstruct the fields everywhere and to compute the impedance of the probe.

In this paper, we consider a conductive piece with a surface varying along a single direction. We will first describe the change of coordinate system and the covariant Maxwell's equations thus obtained. Then, the computational method in the Fourier domain is described. In the last section, the numerical results are presented, discussed and compared with those given by using a finite element software.

1 Formalism

1.1 Change of coordinate system

Let us consider the configuration of Figure 1 where a piece with a bosselated surface is represented and is enlightened by a circular coil. The depth of the interface varies with respect to the x -coordinate and we assume that its analytical equation $z = a(x)$ is known. Let us now apply the following change of variables:

$$\begin{cases} x^1 = x \\ x^2 = y \\ x^3 = z - a(x). \end{cases} \quad (1)$$

In this non-orthogonal coordinate system, although the equation of the interface is simplified, as it becomes $x^3 = 0$, Maxwell's equations become slightly more complicated. Indeed, in order to write them in the new system, we have to introduce the corresponding metric tensor $G = (g_{ij})$.

G takes the following form in our particular coordinates:

$$G = \begin{bmatrix} 1 + (\dot{a}_x)^2 & 0 & \dot{a}_x \\ 0 & 1 & 0 \\ \dot{a}_x & 0 & 1 \end{bmatrix},$$

where $\dot{a}_x = \frac{da}{dx}(x)$.

The inverse tensor, denoted by $G^{-1} = (g^{ij})$, is

$$G^{-1} = \begin{bmatrix} 1 & 0 & -\dot{a}_x \\ 0 & 1 & 0 \\ -\dot{a}_x & 0 & 1 + (\dot{a}_x)^2 \end{bmatrix}.$$

1.2 Physical equations

1.2.1 Covariant Maxwell's equations

Thus, we obtain the so-called covariant Maxwell's equations in each medium (the probe is excluded) which link the covariant components E_c and H_c with the contravariant components D^b and B^b of the electro-magnetic fields:

$$\begin{cases} \partial_b B^b & = 0 \\ \partial_b D^b & = 0 \text{ (no source)} \\ \xi^{abc} \partial_b E_c & = +j\omega B^a \\ \xi^{abc} \partial_b H_c & = (J_p^a + \sigma_p E^a) \end{cases}, a, b, c = 1, 2, 3. \quad (2)$$

These equations are written with the time convention $e^{-j\omega t}$ and the Einstein's convention which are used throughout this paper.

J_p^a denotes the source term in the medium p which is zero in the conductive part and corresponds to the excitation of the probe in air. The terms ξ^{abc} stand for the Lévi-Civita symbol, σ_p is the conductivity of the medium p , ω is the angular frequency, ∂_b stand for the partial derivative with respect to x^b and $j = \sqrt{-1}$. In addition, given the range of frequencies used for ECNDT (10 kHz to 10 MHz) and the usual values of the conductivity ($\simeq 1$ MS/m), the displacement current is neglected.

1.2.2 Constitutive relations of the media

The remaining equalities to be written in the new system are the constitutive relations. They take the following form:

$$\begin{aligned} B^a &= \mu_p H^a = \mu_p \sqrt{g} g^{ab} H_b = \mu_p^{ab} H_b, \\ J^a &= \sigma_p E^a = \sigma_p \sqrt{g} g^{ab} E_b = \sigma_p^{ab} E_b, \\ D^a &= \varepsilon_p E^a = \varepsilon_p \sqrt{g} g^{ab} E_b = \varepsilon_p^{ab} E_b, \end{aligned} \quad (3)$$

where (g^{ab}) is the inverse metric tensor, $g = \det(g^{ab})$, μ_p is the magnetic permeability and ε_p is the electrical permittivity of the medium p .

Here, we can notice that the introduction of the metric tensor can be seen as an artificial anisotropy, because the initial scalar physical constants have all been replaced by tensors. On the other hand, we have seen that the equation of the surface becomes a plane verifying $x^3 = 0$. Thus, the change of coordinate has replaced the complexity of the geometry by complexity of physical properties.

1.2.3 Impedance of the probe

In this NDT configuration (see Fig. 1), we are interested in the computation of the electromagnetic field and the variation ΔZ of the electrical impedance of the probe during a scan over the locally deformed surface. Although other approaches exist, we chose to compute this quantity using the formula derived by Auld and Moulder [7] from the Lorentz reciprocity relation [8]. In the following, ΔZ is the difference of the coil impedance between a reference state (the coil in air for example, or any other configuration...) which can be chosen arbitrarily and the state of interest. We have:

$$I^2 \Delta Z = \iint_{S_F} (\mathbf{E}_a \times \mathbf{H}_b - \mathbf{E}_b \times \mathbf{H}_a) \cdot \mathbf{n} \, ds, \quad (4)$$

where I is the amplitude of the driving current, the subscript a refers to the field generated by the driving coil in the absence of the workpiece (or in a particular configuration of reference as we shall see later), b denotes the field generated by the coil system in the presence of the perturbed workpiece. S_F is an arbitrary closed surface bounding the interface but excluding the coil (see Fig. 2) and \mathbf{n} is the unit outward normal vector, with respect to the closed surface S_F .

For this geometry, S_F is the surface fitting the interface air-conductor. It is closed by a half-cylinder of radius R in the workpiece. Then, let R tends toward infinity. We can now assume that the fields are zero on the cylindrical part of S_F if we are far enough from the coil. Thus, the only remaining term in (4) is the integral on the wavy surface defined by $x^3 = 0$ which will be denoted by S in the following.

1.3 Decomposition and differential formalism

1.3.1 Covariant Helmholtz equations

As it is commonly done when facing a classical electromagnetic problem, we presently work on the covariant Maxwell's equations in order to obtain the Helmholtz

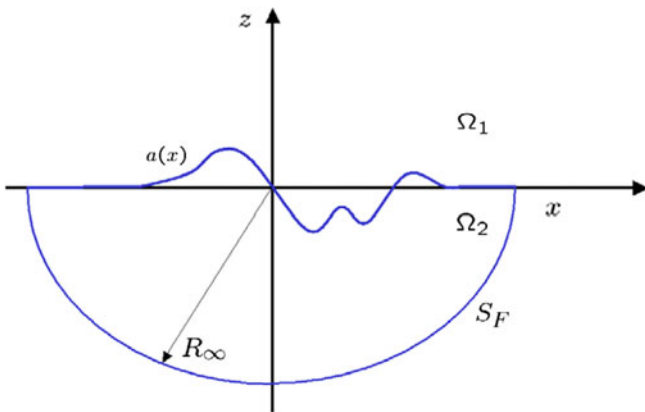


Fig. 2. Definition of the closed surface S_F used in equation (4).

equations for both fields \mathbf{E} and \mathbf{H} . For this purpose, a proper axis decomposition is chosen and we separate the component along x^2 of the two fields from the others. After some tedious calculi, we are finally able to express the remaining components in terms of E_2 and H_2 only and we obtain four coupled partial differential equations in each medium p [6]:

$$\begin{cases} (\partial_2^2 + k_{c_p}^2) E_1^p = \partial_1 \partial_2 E_2^p - j k_{c_p} \left((1 + \dot{a}_x^2) \partial_3 - \dot{a}_x \partial_1 \right) Z_p H_2^p \\ (\partial_2^2 + k_{c_p}^2) E_3^p = \partial_3 \partial_2 E_2^p - j k_{c_p} (\dot{a}_x \partial_3 - \partial_1) Z_p H_2^p \\ (\partial_2^2 + k_{c_p}^2) Z_p H_1^p = \partial_1 \partial_2 Z_p H_2^p + j k_{c_p} \left((1 + \dot{a}_x^2) \partial_3 - \dot{a}_x \partial_1 \right) E_2^p \\ (\partial_2^2 + k_{c_p}^2) Z_p H_3^p = \partial_3 \partial_2 Z_p H_2^p + j k_{c_p} (-\partial_1 + \dot{a}_x \partial_3) E_2^p, \end{cases} \quad (5)$$

with $k_{c_p} = \sqrt{j\omega\mu_p\sigma_p}$, the wave number and $Z_p = \omega\mu_p/k_{c_p}$, the characteristic impedance. Also, the unknowns are reduced to the two components E_2 and H_2 in each medium but we can see in equation (5) that the reconstruction of the other components requires the inversion of the operators $(\partial_2^2 + k_{c_i}^2)$. This operation can be avoided by the substitutions proposed in the next section.

1.3.2 Scalar potentials and final equation

For this purpose, we replace E_2 and H_2 by two scalar potentials and by doing so we remove the inconvenient operator. The two potentials are denoted by Γ and Π and we can define them using E_2 and H_2 as follows:

$$\begin{cases} E_2^p = -j\omega\mu_p \left(\partial_2^2 + k_{c_p}^2 \right) \Gamma^p, \\ H_2^p = \left(\partial_2^2 + k_{c_p}^2 \right) \Pi^p. \end{cases} \quad (6)$$

Finally, we are able to express directly the components along x^1 and x^3 in terms of Γ and Π [9] and we obtain the following expressions where the index p of the medium has been removed for clarity:

$$\begin{cases} E_1 = -j\omega\mu \left(\partial_1 \partial_2 \Gamma + \left(-\dot{a}_x \partial_1 + (1 + \dot{a}_x^2) \partial_3 \right) \Pi \right) \\ E_3 = -j\omega\mu \left(\partial_3 \partial_2 \Gamma + (-\partial_1 + \dot{a}_x \partial_3) \Pi \right) \\ H_1 = \partial_1 \partial_2 \Pi + k_c^2 \left(-\dot{a}_x \partial_1 + (1 + \dot{a}_x^2) \partial_3 \right) \Gamma \\ H_3 = \partial_3 \partial_2 \Pi + k_c^2 (-\partial_1 + \dot{a}_x \partial_3) \Gamma. \end{cases} \quad (7)$$

Finally, these expressions are injected into the covariant Maxwell's equations which can be written in terms of the potentials exclusively. After some calculi, it appears that both potentials verify independently the same equation:

$$\left[c_x \partial_3^2 - (\partial_1 \dot{a}_x + \dot{a}_x \partial_1) \partial_3 + \partial_1^2 + \partial_2^2 + k_c^2 \right] \Gamma = 0, \quad (8)$$

where $c_x = 1 + \dot{a}_x^2$.

Then, if we consider not only Γ and Π in each medium as the unknowns but also $\partial_3 \Gamma$ and $\partial_3 \Pi$, which will be denoted by Γ' and Π' in the following, equation (8) can

be written:

$$\begin{bmatrix} c_x & 0 \\ 0 & 1 \end{bmatrix} \partial_3 \begin{bmatrix} \Gamma' \\ \Gamma \end{bmatrix} = \begin{bmatrix} (\partial_1 \dot{a}_x + \dot{a}_x \partial_1) & -(\partial_1^2 + \partial_2^2 + k_c^2) \\ 1 & 0 \end{bmatrix} \begin{bmatrix} \Gamma' \\ \Gamma \end{bmatrix}. \quad (9)$$

As we will see, from this equation, it is possible to deduce a modal decomposition of the two potentials and their derivatives with respect to x^3 . Indeed, providing some restrictive hypotheses on the solutions, it is possible to turn (9) into an eigenvalue problem.

Besides, at this point it is important to remind the reader that equation (9) is the direct transcription of the Maxwell equations without any source term. As a consequence, once we will be able to compute the proper decomposition of the unknowns, it will depend on the analytical expression of the interface and on the frequency only and it will not be necessary to calculate it again for a displacement of the probe, provided that it is seen as a current source with no interacting part like shielding or ferrite core.

2 Numerical resolution

2.1 Restrictive hypotheses

The first step to solve numerically (9) consists in obtaining numerical operators for all the partial derivatives ∂_k . To do so, we will first apply a 2D-Fourier transform along the axes x^1 and x^2 . The corresponding spatial frequencies will be denoted by u and v , respectively, and by doing so we obtain the Fourier transforms $\hat{\Gamma}$ and $\hat{\Pi}$ of each potential Γ and Π :

$$\hat{\Gamma}(u, v, x^3) = \iint \Gamma(x^1, x^2, x^3) e^{-jx^1 u} e^{-jx^2 v} dx^1 dx^2. \quad (10)$$

Then, in order to obtain a numerical operator for ∂_3 , we assume that the solutions are separable and that their dependency along x^3 is an exponential one, i.e. we focus on solutions taking the form:

$$\begin{cases} \hat{\Gamma}(u, v, x^3) = \hat{\Psi}(u, v) \exp(j\lambda x^3) \\ \frac{\partial \hat{\Gamma}}{\partial x^3}(u, v, x^3) = \hat{\Phi}(u, v) \exp(j\lambda x^3). \end{cases} \quad (11)$$

With all these hypotheses, we are able to re-write equation (9) and we obtain the following eigenvalue system in Fourier domain:

$$\begin{bmatrix} \hat{C} & 0 \\ 0 & 1 \end{bmatrix} \lambda \begin{bmatrix} \hat{\Phi}(u, v) \\ \hat{\Psi}(u, v) \end{bmatrix} = \begin{bmatrix} (u\hat{A} + \hat{A}u) & j\beta^2 \\ -j & 0 \end{bmatrix} \begin{bmatrix} \hat{\Phi}(u, v) \\ \hat{\Psi}(u, v) \end{bmatrix}, \quad (12)$$

where $\beta^2 = k_c^2 - u^2 - v^2$.

The matrices \hat{A} and \hat{C} stand for the convolution operator with $TF(\dot{a}_x)$ and $TF(c_x)$, respectively, as a product in the spatial domain is transformed into a convolution in the spectral domain.

2.2 Modal decomposition

The eigenvalue system (12) is solved once for each value of the spatial frequency v (corresponding to the direction x^2). The resolution of (12) allows us to express the two potentials and their derivatives as linear expansions of eigenvectors in each medium p and for each v :

$$\begin{aligned} \hat{\Gamma}^{(p)} &= \sum_q \psi_{q,p}^+ \Gamma_{q,p}^+ e^{j\lambda_{q,p}^+ x^3} + \sum_q \psi_{q,p}^- \Gamma_{q,p}^- e^{j\lambda_{q,p}^- x^3}, \\ \frac{\partial \hat{\Gamma}^{(p)}}{\partial x^3} &= \sum_q \phi_{q,p}^+ \Gamma_{q,p}^+ e^{j\lambda_{q,p}^+ x^3} + \sum_q \phi_{q,p}^- \Gamma_{q,p}^- e^{j\lambda_{q,p}^- x^3}, \\ \hat{\Pi}^{(p)} &= \sum_q \psi_{q,p}^+ \Pi_{q,p}^+ e^{j\lambda_{q,p}^+ x^3} + \sum_q \psi_{q,p}^- \Pi_{q,p}^- e^{j\lambda_{q,p}^- x^3}, \\ \frac{\partial \hat{\Pi}^{(p)}}{\partial x^3} &= \sum_q \phi_{q,p}^+ \Pi_{q,p}^+ e^{j\lambda_{q,p}^+ x^3} + \sum_q \phi_{q,p}^- \Pi_{q,p}^- e^{j\lambda_{q,p}^- x^3}, \end{aligned} \quad (13)$$

where $\psi_{q,p}^\pm$ and $\phi_{q,p}^\pm$ are the eigenvectors associated to the eigenvalue $\lambda_{q,p}^\pm$ and $\Gamma_{q,p}^\pm$ and $\Pi_{q,p}^\pm$ are the unknown coefficients. The \pm exponents are used to separate the progressive and the regressive contributions. Indeed, we have obtained a mathematical solution of Maxwell's equations but to make it physically acceptable, it is necessary to add the outgoing wave condition. To do so, we will remove all the terms growing as we move toward infinity. In other words, all the eigenvectors corresponding to $\Im m(\lambda) < 0$ in air ($x^3 \rightarrow +\infty$) and $\Im m(\lambda) > 0$ in the piece ($x^3 \rightarrow -\infty$) must be suppressed.

2.3 Numerical Fourier transform and truncature

Up to now, we have considered continuous spectral axes u and v (the modal decomposition has an infinite number of terms). However, in order to compute the Fourier transform (10), it is necessary to discretize the 2D spectral domain and to bind it. If we denote by $2M_u + 1$ and $2M_v + 1$ the number of discrete spatial frequencies along the two axes, it can be shown that we will obtain exactly $N = (2M_u + 1)(M_v + 1)$ different eigenvalues. As it is clear that the accuracy of the modal expansion relies on the number of terms, we want to emphasize here the important role of these numbers for this method.

The number of frequencies or spectral modes being fixed, it is necessary to choose the spatial sample periods T_x and T_y . Two criteria are considered: the derivative of the interface has to be well-represented in Fourier-domain as well as the incident fields we will soon introduce. In other words, the spectral parameters have to be so chosen that the numerical $TF(TF^{-1})$ operation does not affect the profile or the source terms.

2.4 Boundary conditions and reconstruction

2.4.1 Physical boundary conditions

At this point, the coefficients $\Gamma_{q,p}^\pm$ and $\Pi_{q,p}^\pm$ of the decomposition are to be determined by adding the boundary

conditions on the interface. Indeed, we have to ensure the continuity of the tangential components of the fields \mathbf{E} and \mathbf{H} across the rough surface, whose equation is simply $x^3 = 0$, thanks to the spatial transformation operated. The tangential components are E_1 , E_2 , H_1 and H_2 . Moreover, we have to introduce here the incident field, i.e. the one created by the probe in an open space which can be evaluated analytically. We obtain the following equality:

$$\underbrace{\begin{bmatrix} E_1^{(inc)} \\ E_2^{(inc)} \\ H_1^{(inc)} \\ H_2^{(inc)} \end{bmatrix}}_{\text{air}} + \underbrace{\begin{bmatrix} E_1^{(R)} \\ E_2^{(R)} \\ H_1^{(R)} \\ H_2^{(R)} \end{bmatrix}}_{\text{conductor}} \stackrel{x^3=0}{=} \underbrace{\begin{bmatrix} E_1^{(T)} \\ E_2^{(T)} \\ H_1^{(T)} \\ H_2^{(T)} \end{bmatrix}}_{\text{conductor}}. \quad (14)$$

Although this formulation is physically correct, it has a drawback: the fields created by a coil alone present a wide spatial expansion and would require a large number of spatial frequencies to be well represented. As a consequence, this leads to a large eigenvalue system which deteriorates the efficiency of the code.

The solution we have chosen consists in using a relative reference with a smaller spatial expansion. We choose to use the fields created by the probe enlightening a plane conductor located at the inferior depth of the rough surface and to interpolate it on the effective surface. This field is given by a semi-analytical model implemented in the Civa platform [10,11] developed at the Cea List. The refracted field calculated in this way stands now as a perturbation term. We have, for example:

$$\underbrace{E_{\text{air}}^{(inc)} + E_{\text{plane}}^{(R)}}_{\text{reference}} + \underbrace{E^R - E_{\text{plane}}^{(R)}}_{\text{perturbation}} \stackrel{x^3=0}{=} E^T. \quad (15)$$

2.4.2 Numerical implementation

Finally, by using relations (7) in the Fourier domain, we can replace the unknown refracted and transmitted fields by their expression in terms of the potentials in each medium. As for the potentials $\Gamma^{(p)}$ and $\Pi^{(p)}$ and their derivatives with respect to x^3 , they are replaced by their corresponding modal expansion (see Sect. 1.3). The boundary system is implemented for each value of the spatial frequency v (and all the frequencies u at once) and leads to four matrix equations. The numerical operators are defined as follows:

$$\begin{aligned} \mathcal{M}^{(p)} &= -j\omega\mu_p [jv j\mathbf{u}\psi_p], \\ \mathcal{N}^{(p)} &= -j\omega\mu_p \left[-\hat{A}j\mathbf{u}\psi_p + \hat{C}\phi_p \right], \\ \mathcal{O}^{(p)} &= -j\omega\mu_p \left[(jv)^2 + k_{c_p}^2 \right] \psi_p, \\ \mathcal{P}^{(p)} &= k_{c_p}^2 \left[-\hat{A}j\mathbf{u}\psi_p + \hat{C}\phi_p \right], \\ \mathcal{Q}^{(p)} &= [jv j\mathbf{u}\psi_p], \\ \mathcal{R}^{(p)} &= \left[(jv)^2 + k_{c_p}^2 \right] \psi_p, \end{aligned} \quad (16)$$

where ψ_p and ϕ_p are vectors containing the eigenvectors in each medium and \mathbf{u} is a diagonal matrix containing all

the spatial frequencies along x^1 . Using (6), (7), (14) and (16), we can write the four boundary conditions in the following form:

$$\begin{aligned} \mathcal{M}^{(1)}\Gamma_1^- + \mathcal{N}^{(1)}\Pi_1^- - \mathcal{M}^{(2)}\Gamma_2^+ - \mathcal{N}^{(2)}\Pi_2^+ &= -\mathbf{E}_1^{(ref)}, \\ \mathcal{O}^{(1)}\Gamma_1^- - \mathcal{O}^{(2)}\Gamma_2^+ &= -\mathbf{E}_2^{(ref)}, \\ \mathcal{P}^{(1)}\Gamma_1^- + \mathcal{Q}^{(1)}\Pi_1^- - \mathcal{P}^{(2)}\Gamma_2^+ - \mathcal{Q}^{(2)}\Pi_2^+ &= -\mathbf{H}_1^{(ref)}, \\ \mathcal{R}^{(1)}\Pi_1^- - \mathcal{R}^{(2)}\Pi_2^+ &= -\mathbf{H}_2^{(ref)}, \end{aligned} \quad (17)$$

where the exponent (*ref*) stands for the fields calculated considering a plane configuration as they were introduced in (15) and Γ_p^\pm and Π_p^\pm are vectors containing all the unknown coefficients in each medium. For each v , (17) is a system of $4 \times (2M_u + 1)$ equations and its inversion leads to the determination of the $4 \times (2M_u + 1)$ unknown coefficients.

Once the coefficients are calculated, the tangential components of the fields on the boundary in the media p are easily computed using the same operators applied to the corresponding coefficients. The normal components are obtained in the same way since using (8) leads to the following expression in Fourier domain:

$$\begin{aligned} E_3^p &= -j\omega\mu_p \left[jv\phi_p \Gamma_p^\pm + \left(\hat{A}\phi_p - j\mathbf{u}\psi_p \right) \Pi_p^\pm \right] \\ &\quad \text{and} \\ H_3^p &= jv\phi_p \Pi_p^\pm + k_{c_p}^2 \left(\hat{A}\phi_p - j\mathbf{u}\psi_p \right) \Gamma_p^\pm. \end{aligned}$$

In air, the complete solution is the sum of the reconstructed perturbation and the reference whereas, in the piece, the reconstruction leads directly to the determination of the complete transmitted fields. From its value on the surface, the field in both media can be easily evaluated everywhere by multiplying the operators detailed in (16) with a vector containing the exponential terms of the expansion (13) stored in the same order as the coefficients and eigenvectors.

2.5 Computation of the impedance

To supplement the solution of the C method and to prepare a future comparison with experimental data, it is necessary to compute the impedance of the probe since it is the typical signal obtained during a real scan. For this purpose, we use the approach presented in Section 1.2.3 where we introduced the closed surface S_F and the interface air-conductor S .

It was shown that the closed integral over S_F (4) is equivalent to the integral over S , providing that the bounds of the interface are sufficiently far from the source to ensure that the fields are zero on the cylindrical part of S_F . Besides, the superscript a refers to the fields calculated with a plane located at the extreme depth of the profile, which is the configuration we used as a reference when applying the boundary conditions (see Sect. 2.4). b denotes the total field in the presence of the perturbed conductor. As a consequence, ΔZ represents here the variation of the total electrical impedance in comparison with the plane configuration (reference): $\Delta Z = Z_{total} - Z_{plane}$.

The cross product of the fields is calculated from the Cartesian components and the projection on the normal direction is then performed. Using the change of coordinate system introduced in Section 1.1, it can be shown that the normal component of any vector \mathbf{F} is the contravariant component along x^3 , commonly denoted by F^3 (the position of the superscript does matter here). This component can be expressed in terms of the Cartesian components and we have: $F^3 = (-\dot{a}_x F_x + F_z) / \sqrt{1 + \dot{a}_x^2}$. We can finally express this component in terms of the covariant components only and finally, we obtain:

$$(\mathbf{E} \times \mathbf{H}) \mathbf{n} = \frac{E_1 H_2}{\sqrt{1 + \dot{a}_x^2}}.$$

To obtain the absolute impedance, it is necessary to sum the result ΔZ with the impedance of the plane configuration calculated by the same semi-analytical model used for the computation of the reference fields.

3 Numerical results and validations

3.1 Configuration

The particular configuration considered for the validation of the method is presented in Figure 3 and its characteristic parameters are stored in Table 1. The wavy shape is assumed to be a part of a cosine function, expressed analytically as follows:

$$a(x) = \begin{cases} -\frac{h_p}{2} \left(1 + \cos \left(2\pi \frac{x}{L_p} \right) \right), & \forall x \in [-L_p/2, L_p/2] \\ 0, & \text{elsewhere.} \end{cases}$$

This particular function has been chosen for its smoothness, but any analytical function can be chosen, as long as the Fourier transform of its first derivative is numerically tractable. The probe considered is a cylindrical pancake coil with a rectangular cross-section. For the first validation presented here, it has been placed directly above the geometrical perturbation.

3.2 Results

For the validation of our method, we use a commercial FE solver (Comsol multiphysics [12]) to calculate the fields inside the workpiece. This software gives us the components

Table 1. Parameters of the configuration used for the validation.

Parameter	Symbol	Value
Conductor		
Conductivity	σ	1 MS/m
Depth of the shape	h_p	1.2 mm
Length of the shape	L_p	10 mm
Probe		
Frequency	f	50 kHz
Excitation current	I_0	1 ampere
Internal radius	r_{int}	1.0 mm
External radius	r_{ext}	1.6 mm
Height	H	2 mm
Liftoff	l_0	0.3 mm

of the fields in the Cartesian system on a predefined mesh. Since we intend to compare the covariant components in the workpiece, the solutions are transformed by using the change of basis formulas presented in Section 1.1. Both solutions have been computed on two surfaces $x^3 = \text{constant}$ in the depth of the conductive piece. We present here the most representative components, i.e. those which are the most altered by the presence of the local perturbation. The results presented here have been obtained with the numerical parameters stored in Table 2.

As a consequence, we have solved $2M_v + 1 = 31$ eigenvalue and boundary conditions (i.e., matrix inversion) problems of size $2M_u + 1 = 51$ and $4(2M_u + 1) = 204$ respectively. The time of computation with these parameters and without the calculus of the reference field (which is considered as an entry for the model) is 4.5 s on a 64-bit platform.

In Figures 4–7 we have represented the cartographies of the real and imaginary parts of E_1 , H_1 , E_3 and H_2

Table 2. Numerical parameters used for the validation.

Parameter	Symbol	Value
Number of modes along x^1	M_u	25
Spatial bound along x^1	x_{max}	20 mm
Sample period along x^1	T_x	0.0783 mm
Number of modes along x^2	M_v	15
Spatial bound along x^2	y_{max}	20 mm
Sample period along x^2	T_y	0.0783 mm

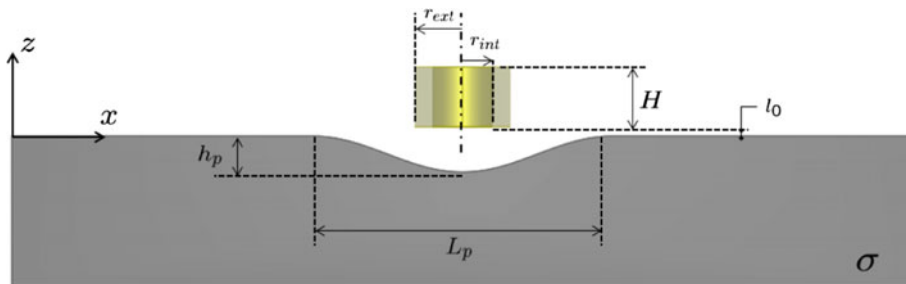


Fig. 3. Configuration for the validation.

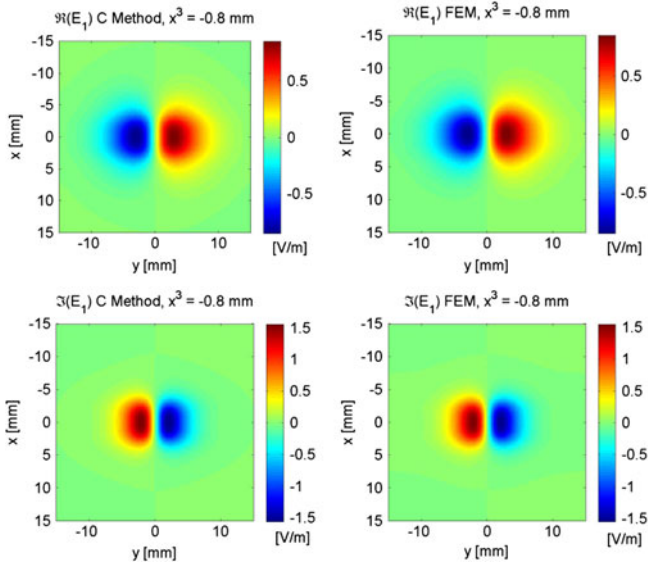


Fig. 4. Real and imaginary parts of the E_1 component of the magnetic field, computed on the surface $x^3 = -0.8$ mm.

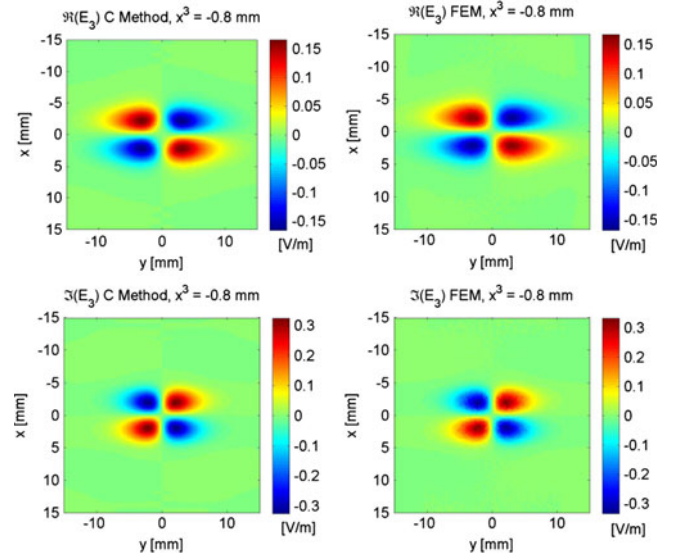


Fig. 6. Real and imaginary parts of the E_3 component of the electric field, computed on the surface $x^3 = -0.8$ mm.

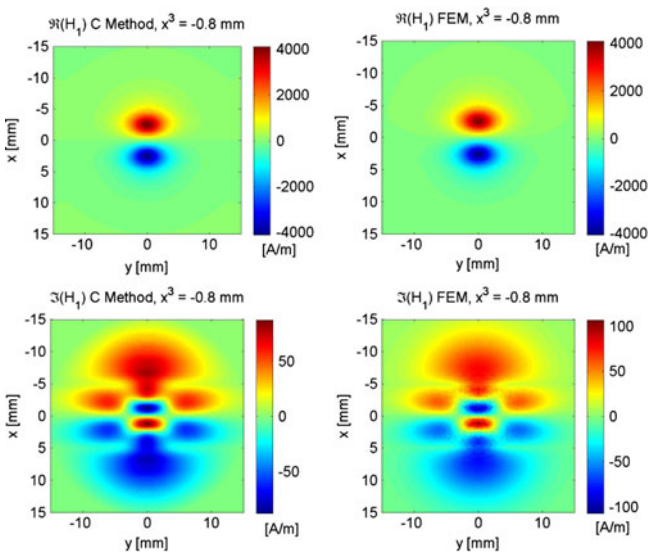


Fig. 5. Real and imaginary parts of the H_1 component of the magnetic field, computed on the surface $x^3 = -0.8$ mm.

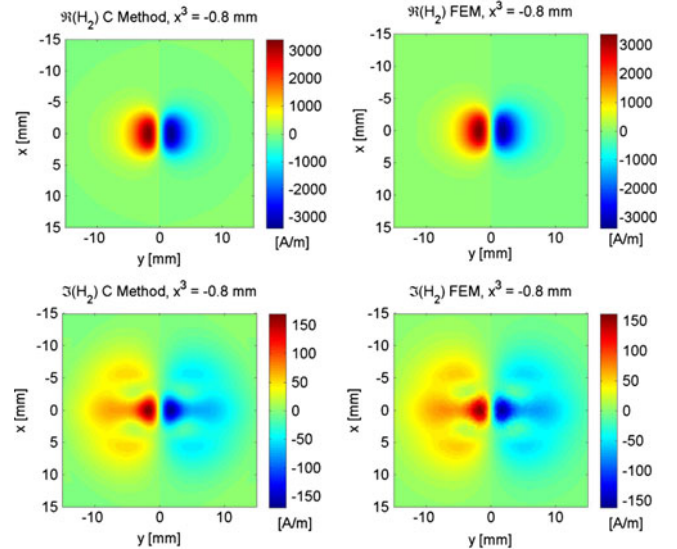


Fig. 7. Real and imaginary parts of the H_2 component of the magnetic field, computed on the surface $x^3 = -0.8$ mm.

respectively. These solutions have been computed using the two methods (C method and FEM) on the surface $x^3 = -0.8$ mm. Those components are the most altered by the perturbation (compared to a plane geometry), particularly E_3 which is zero in the case of a plane conductor. Qualitatively, results given by the C method are close to the FEM solution, as we can notice that they have the same form and their amplitudes appear similar.

In order to make a more accurate comparison of the amplitudes of the fields and to verify that they are properly calculated everywhere in the piece, we have represented the real and imaginary parts of the components E_1 , E_3 , H_1 and H_2 along the most relevant sections ($x =$

constant or $y =$ constant). These components are evaluated in the conductor on two surfaces “parallel” to the interface $x^3 = 0$, namely $x^3 = -0.4$ and -0.8 mm. The plots obtained are represented in Figures 8–11.

We can notice a good agreement between the two solutions which confirms that the fields are well computed everywhere in the conductive piece. The low differences are most likely due to the necessary bounding of the two domains (air and conductor) for the FEM computation: the radiation condition of the field at infinity is approximated by applying Dirichlet conditions on the edges of the box and can be a source of inaccuracy. Besides, the density of the mesh is limited by the internal memory of the computer we used to compute the FEM solution.

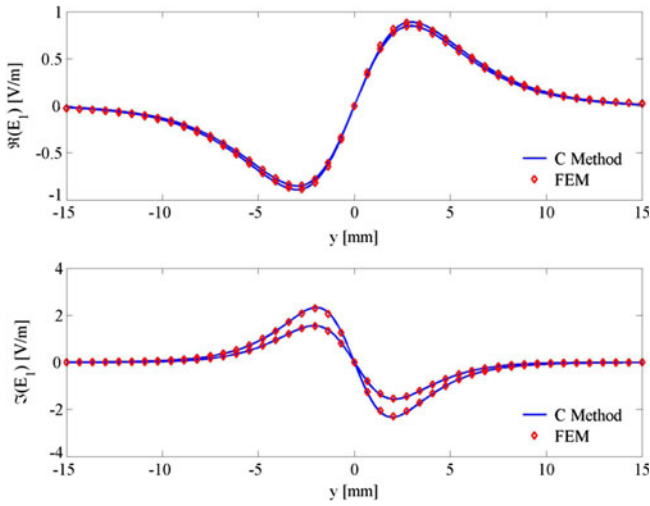


Fig. 8. Real and imaginary parts of the component E_1 represented along the section $x = 0$ for the two surfaces $x^3 = -0.4$ mm and $x^3 = -0.8$ mm.

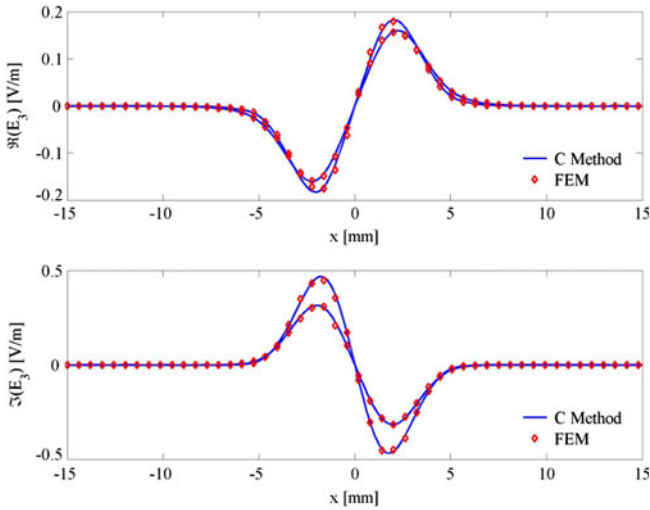


Fig. 9. Real and imaginary parts of the E_3 component, represented along the section $y = 2.5$ mm for the two surfaces $x^3 = -0.4$ mm and $x^3 = -0.8$ mm.

An improvement of the results is thus very likely to be observed with a finer mesh and a larger domain.

In order to quantify the error between the simulated datas provided by each model (method C and FEM), we have computed the quadratic relative error defined as follows:

$$\xi = \sqrt{\frac{\|F_{\text{FEM}} - F_{\text{Cmethod}}\|^2}{\|F_{\text{FEM}}\|^2}}, \quad (18)$$

where $\|\cdot\|$ stands for the euclidean norm and F refers to one of the covariant components of the fields at the depth of interest. The error on each component of fields \mathbf{E} and \mathbf{H} has been computed for each depth of observation. The results are presented in Table 3 for the electrical field and Table 4 for the magnetic field.

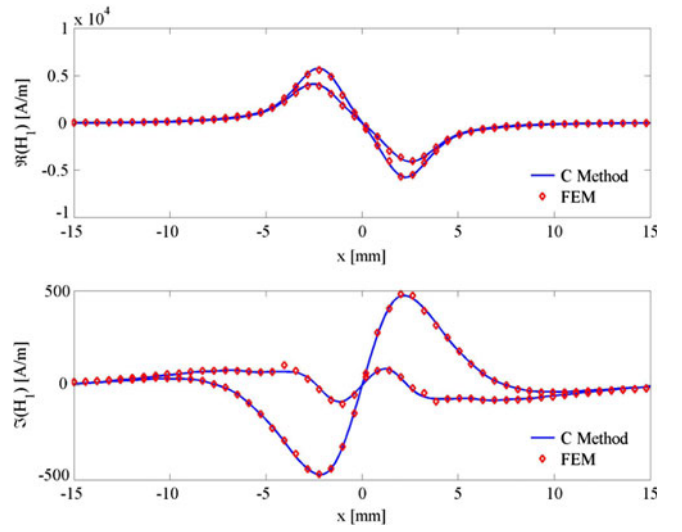


Fig. 10. Real and imaginary parts of the H_1 component, represented along the section $y = 0$ for the two surfaces $x^3 = -0.4$ mm and $x^3 = -0.8$ mm.

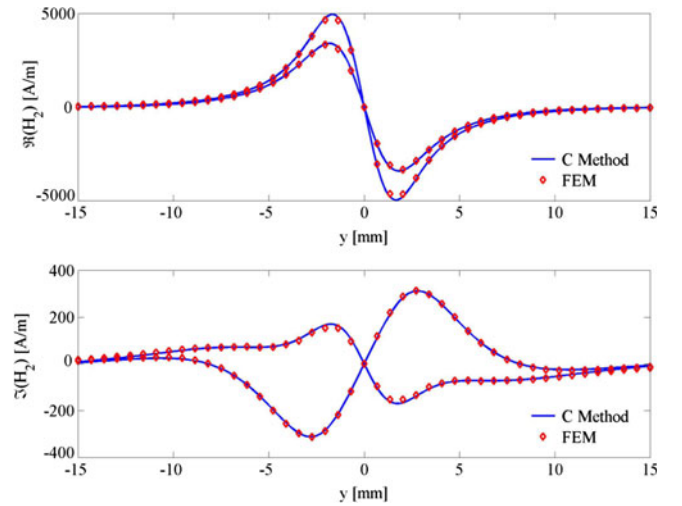


Fig. 11. Real and imaginary parts of the H_2 component, represented along the section $x = 0$ for the two surfaces $x^3 = -0.4$ mm and $x^3 = -0.8$ mm.

Table 3. Quadratic relative error in % on the electric field.

Depth (mm)	$\xi(\%) E_1$	$\xi(\%) E_2$	$\xi(\%) E_3$
0.4	2.43	2.93	5.34
0.8	2.16	2.64	6.27
1.2	1.96	2.42	4.48

First, we can remark that the errors are growing when moving toward the interface because the fields are more intense and their variations more significant close to the surface. As a consequence, because the density of the mesh remains equal when moving downward, it seems very likely that the fields are better calculated in depth. The mean

Table 4. Quadratic relative error in % on the magnetic field.

Depth (mm)	$\xi(\%) H_1$	$\xi(\%) H_2$	$\xi(\%) H_3$
0.4	3.60	2.50	3.61
0.8	3.14	2.32	3.30
1.2	2.83	2.10	2.98

Table 5. Real part of the coil impedance calculated at different frequencies with FEM and C method respectively and the relative error.

Frequency (kHz)	$\Re(Z_{\text{FEM}})$	$\Re(Z_{\text{C}_{\text{method}}})$	$\xi\% \Re(Z)$
50	0.449	0.453	0.89
100	1.035	1.047	1.16
150	1.60	1.62	1.25

Table 6. Imaginary part of the coil impedance calculated at different frequencies with FEM and C method respectively and the relative error.

Frequency (kHz)	$\Im(Z_{\text{FEM}})$	$\Im(Z_{\text{C}_{\text{method}}})$	$\xi\% \Im(Z)$
50	56.39	56.29	0.18
100	112.30	112.44	0.12
150	167.97	168.50	0.31

error (ξ) on the different components is equal to 3.57% for this configuration.

To complete the validation of the model, the impedance of the sensor for three different frequencies (50, 100 and 150 kHz) has been computed with the two methods and the errors have been calculated in the same way as before. The real parts of the impedance are stored in Table 5 and the imaginary parts in Table 6. We can see that the relative error is around 1% for the real part and 0.3% for the imaginary part.

All these comparisons and low errors obtained highlight the validity of the numerical model. Moreover, the computation time is very low.

4 Conclusion

In this paper, the validity and the efficiency of the C method for the fields and impedance calculation above an unflawed piece in a 2.5D configuration has been demonstrated for the first time (the workpiece is 2D while the EC probe is 3D). A relatively general formalism has been described as well as its implementation in a numerical model. This fast semi-analytical solver has been validated, for a particular configuration, through the comparison with a FEM commercial solver and appeared accurate. The main purpose of this paper is to show the validity of such an

approach as well as its flexibility. Indeed, the generality of the theory presented here proves the large number of its applications in NDT especially for perturbed shapes as the only theoretical hypotheses we made on the function representing the irregularity are that its spatial Fourier transform does exist. Besides, we have seen that the reference field is an external input to this model and can be computed by any solver able to evaluate the fields induced by a sensor in air above a plane conductor. This important particularity shows the validity of the method for any air-core NDT probe if we are able to compute the fields for a plane geometry and thus enlarges the number of applications.

Preliminary developments described in this paper may be completed by many extensions. First of all, the influence of the spectral parameters on the convergence will be studied. Then, a scan of the piece will be simulated by moving the coil along the local perturbation. Afterwards, other shapes and other probes will be tackled. Finally, the numerical model will be extended in order to be able to treat the very interesting cases of a plate and a stratified conductor constituted by a number of layers with rough interfaces.

The research leading to these results has received funding from the European Community's Seventh Framework Program (FP7/2007-2013) under Grant Agreement No. 285549: SIM-POSIUM project.

References

1. O. Michelsson, F. Ulmann, IEEE Trans. Magn. **36**, 756 (2000)
2. J. Chandezon, D. Maystre, G. Raoult, J. Optics **11**, 235 (1980)
3. L. Li, J. Chandezon, G. Granet, J. Plumey, Appl. Opt. **38**, 304 (1999)
4. D. Prémel, J. Phys. D: Appl. Phys. **41**, 245305 (2008)
5. E. Post, *Formal Structure of Electromagnetics: General Covariance and Electromagnetics* (Dover Publications Inc., North-Holland, Amsterdam, 1962)
6. K. Braham, R. Dusséaux, G. Granet, Waves Random Complex Media **18**, 255 (2008)
7. B. Auld, J. Moulder, J. Nondestr. Eval. **18**, 3 (1999)
8. R. Collin, *Foundations for Microwaves Engineering* (McGraw-Hill, New York, 1992)
9. D. Prémel, J. Electromagnetic Analysis and Applications **4**, 400 (2012)
10. C. Dodd, W. Deeds, J. Appl. Phys. **39**, 2829 (1968)
11. C. Reboud, T. Theodoulidis, Stud. Appl. Electromagn. Mech. **36**, 3 (2012)
12. Comsol multiphysics v4.2 user's guide, <http://www.comsol.com/>, 2011.